ChemComm

COMMUNICATION

View Article Online
View Journal



Cite this: DOI: 10.1039/d5cc07385e

Received 29th December 2025,
Accepted 12th April 2026

DOI: 10.1039/d5cc07385e

rsc.li/chemcomm

# Selective ammonia sensing through reversible vapochromism and luminescence ON–OFF switching of a chalcone-based Co(II) complex

Mai Mukoyama,[a] Masashi Hashimoto,[ab] Yuta Shudo,[c] Hajime Yagi,[ab] Hayato Kikuchi[a] and Manabu Nakaya*[ab]

**In this work, a chalcone-based cobalt(II) complex exhibits ammonia ($NH_3$)-induced vapochromism with reversible luminescence ON–OFF switching, triggered by partial dissociation and $NH_3$ insertion at the cobalt(II) center.**

Stimuli-responsive metal complexes that exhibit optical changes have emerged as a key class of materials for applications in chemosensing, bioimaging, and smart optical devices.[1–5] Reversible modulation of the coordination environment and metal oxidation state at the metal center—as well as subtle changes in molecular arrangement within the crystal lattice—provides a versatile platform for constructing systems capable of physically- or chemically-induced electronic or spin switching.[6–10] Optically active compounds based on such mechanisms have been widely investigated for sensing industrially relevant gases ($O_2$, $CO_2$, $N_2$, *etc.*) as well as environmentally hazardous gases and pollutants ($NO_x$, $SO_x$, $NH_3$) and other volatile organic compounds (VOCs).[11–14]

Polymeric solid materials such as metal–organic frameworks (MOFs), inorganic perovskites and so on have long been explored as highly effective guest adsorbents, owing to their stable porosity and high surface areas.[15–19] However, translating adsorption events into clear and readily observable physical responses remains challenging. As a result, systems that enable direct and instantaneous optical readouts for *in situ* sensing remain relatively limited.[20,21] In recent years, however, discrete metal complexes have attracted increasing attention as promising candidates for sensing, particularly industrially relevant gases and pollutants.[22–26] These studies underscore the broad applicability of coordination-driven switching mechanisms for the selective and sensitive detection of diverse chemical analytes. On the other hand, molecular compounds can exhibit much faster and more discrete structural or optical changes, yet they typically suffer from limited chemical selectivity toward specific analytes.

Herein, we report a mononuclear cobalt(II) complex bearing a chalcone-based luminescent ligand (**L1·Co**) that exhibits highly selective and reversible vapochromism and luminescence ON–OFF switching in response to ammonia ($NH_3$) vapor. The switching mechanism involves partial dissociation of the ligand upon $NH_3$ coordination to the Co(II) center, restoring the ligand's intrinsic emission. Subsequent removal of $NH_3$ leads to reformation of the original **L1·Co** and quenching of the luminescence. These reversible optical changes are supported by reflectance spectroscopy, powder X-ray diffraction (PXRD), gas adsorption analysis, elemental analysis and density functional theory (DFT) calculations.

The luminescent ligand **L1**, a chalcone derivative bearing a dimethylamine group, was synthesized according to a reported procedure with minor modifications (see Experimental section in the SI).[27] Single crystals of **L1·Co** suitable for single crystal X-ray diffraction (SC-XRD) were obtained by slow evaporation of an acetone solution of **L1** and $CoCl_2{\cdot}4H_2O$ (Fig. 1), enabling detailed elucidation of the coordination environment at the metal center. Crystallographic parameters are summarized in Table S1. Elemental analysis indicated the presence of a small amount of adsorbed solvent in the powder sample (Table S2); however, the PXRD pattern was consistent with that simulated from the SC-XRD data. This result suggests that the detected solvent molecules are surface-adsorbed, as no lattice solvent molecules were observed in the crystal structure. Notably, the powder sample of **L1·Co** is structurally identical to the crystalline sample; therefore, it was used in most subsequent experiments.

Solid-state reflectance spectra of **L1** (green dashed line) and **L1·Co** (red solid line) are shown in Fig. 2a. The reddish-brown **L1** ligand exhibited a decrease in reflectance below 600 nm, whereas its cobalt(II) complex **L1·Co**, with a darker brown color, showed reduced reflectance extending to below 800 nm. This reflectance change upon metal complexation, *i.e.*, red-shift in

[a] *Department of Material Science, Graduate School of Science, Josai University, 1-1 Keyakidai, Sakado, Saitama 350-0295, Japan. E-mail: nakaya@josai.ac.jp*
[b] *Department of Chemistry and Biological Science, Faculty of Science, Josai University, 1-1 Keyakidai, Sakado, Saitama 350-0295, Japan*
[c] *Nanomaterials Research Institute, National Institute of Advanced Industrial Science and Technology (AIST), 1-1-1 Higashi, Tsukuba 305-8565, Japan*

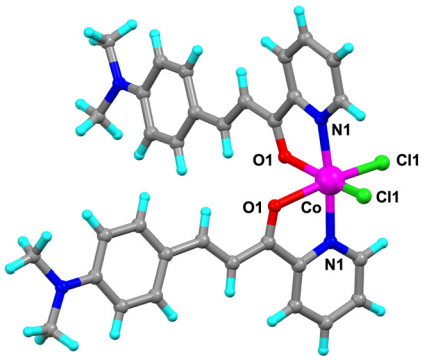


Fig. 1 Crystal structure of **L1·Co**. Color code: C, grey; N, blue; H, light blue; O, red; Cl, green; Co, magenta.

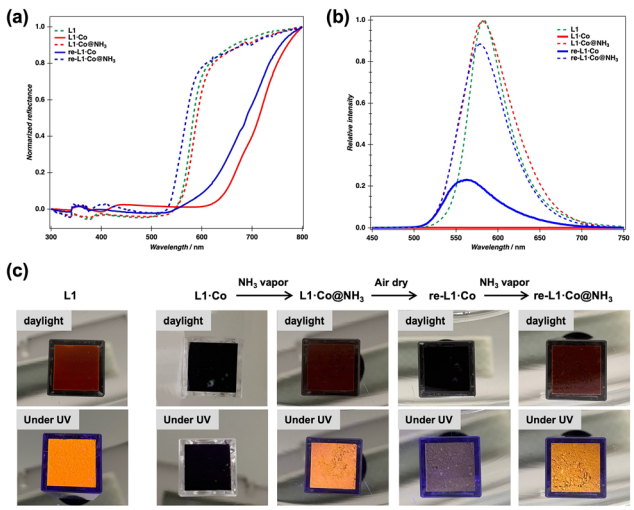


Fig. 2 (a) Normalized reflectance spectra and (b) luminescence spectra of **L1** (green dashed line), **L1·Co** (red solid line), **L1·Co@NH$_3$** (red dashed line), **re-L1·Co** (blue solid line) and **re-L1·Co@NH$_3$** (blue dashed line). (c) Photographs of powder samples of **L1**, **L1·Co**, **L1·Co**, **L1·Co@NH$_3$**, **re-L1·Co**, and **re-L1·Co@NH$_3$** (left to right) in a cuvette under daylight (top) and UV light (bottom).

absorption, is attributed to metal-to-ligand charge transfer (MLCT). As shown in Fig. 2b, the luminescence spectrum of **L1** (green dashed line) displays a clear emission maximum at 585 nm ($\lambda_{ex}$ = 405 nm), whereas **L1·Co** exhibits no detectable emission (red solid line).

The optical response of **L1·Co** to $NH_3$ vapor (generated from a 28% aqueous $NH_3$ solution) was investigated. Upon exposure of a powder sample of **L1·Co** in a cuvette to $NH_3$ vapor, the dark brown color immediately changed to reddish-brown, and the resulting state is denoted as **L1·Co@NH$_3$** (Fig. 2c). Notably, **L1·Co@NH$_3$** exhibited orange luminescence under UV irradiation, whereas pristine **L1·Co** showed no detectable emission (middle photographs in Fig. 2c). After air-drying **L1·Co@NH$_3$** for a few minutes, the color reverted to the original dark brown state (**re-L1·Co** in Fig. 2c). Re-exposure to $NH_3$ vapor reproducibly induced the same optical changes, yielding **re-L1·Co@NH$_3$**. Although the emission intensity of **re-L1·Co** does not completely return to the original baseline after the recovery step, the ON–OFF switching remains clearly distinguishable. The residual emission is attributed to incomplete removal of $NH_3$ from the solid state, consistent with elemental analysis indicating trace $NH_3$ remaining after drying (see below).

The reproducibility of the switching behavior over repeated $NH_3$ exposure and drying cycles is shown in Fig. S1. Although the ON/OFF ratio was slightly decreased, reversibility was confirmed for at least three cycles. The reversible response can be attributed to $NH_3$ molecules, as no color or luminescence change was observed when **L1·Co** was exposed to water vapor under identical experimental conditions (Fig. S2). Furthermore, **L1·Co** exhibited high selectivity toward $NH_3$ over other volatile organic solvents and amines, which can be rationalized by the strong coordination affinity of ammonia and its small molecular size. A visually detectable luminescence response was maintained down to 1 wt% aqueous ammonia. This corresponds to an estimated $NH_3$ vapor concentration of *ca.* 8600 ppm under ambient conditions (based on Henry's law[28]). While this detection limit does not reach the sub-ppm levels reported for some porous or device-based sensors, the present system offers distinct advantages as a structurally defined discrete molecular metal complex, enabling reversible coordination-driven switching with a direct optical readout clearly observable to the naked eye.

The changes in color and luminescence feature of **L1·Co** before and after exposure to $NH_3$ vapor were further examined by optical spectroscopic measurements, as summarized in Fig. 2a and b. The reflectance spectrum of **L1·Co@NH$_3$** (red dashed line) is nearly identical to that of **L1** (green dashed line). This observation implies that the coordination environment formed between the cobalt(II) center and the **L1** ligand is disrupted upon $NH_3$ insertion,[29] resulting in the generation of free **L1**. Consistent with this interpretation, the luminescence feature of **L1·Co@NH$_3$** (red dashed line) is recovered upon exposure to $NH_3$ vapor. Upon air-drying **L1·Co@NH$_3$**, the reflectance spectrum of **re-L1·Co** (blue solid line) again exhibits a red-shift, indicating partial removal of coordinated $NH_3$ molecules and the reformation of the original metal–ligand coordination environment. Associated with this process, the luminescence intensity decreases again (blue solid line); however, it does not completely vanish and exhibits a slight spectral shift. This behavior is attributed to residual $NH_3$ molecules remaining in the solid, which leads to incomplete dissociation of the original coordination environment. As a result, reversible luminescence ON–OFF switching is clearly observed upon alternating exposure to $NH_3$ vapor and air-drying (blue dashed line).

To reactivate the luminescence feature, partial dissociation of the **L1** ligand from the Co(II) center is required. Metal complexes containing unpaired spins, such as cobalt(II) complex **L1·Co**, are generally prone to luminescence quenching due to efficient nonradiative relaxation pathways. Even if only the chloride (Cl) atoms coordinated to the Co(II) center are replaced by $NH_3$ molecules, nonradiative relaxation is still expected to remain operative. However, if **L1** ligands were to be completely removed from the Co(II) center, *i.e.*, decomposition of the metal complex formation, re-complexation in the solid-state would be difficult to achieve. Thus, $NH_3$ molecules are likely to be partially inserted through

dissociation of the coordination bonds involving the pyridine N atoms, whose coordination donor ability is reduced by the electron-withdrawing effect of the adjacent carbonyl group.[30]

To clarify this hypothesis, density functional theory (DFT) structural optimizations and time-dependent DFT (TD-DFT) calculations at the B3LYP[31] theoretical level were performed using the Gaussian 16 program[32] with the 6-311G(d,p) basis sets for all other atoms. The absorption of the **L1** ligand is attributed to an intra-ligand charge transfer (ILCT) from the dimethylaminophenyl moiety to the carbonyl-pyridine site (Fig. S3). In contrast, both **L1·Co** and **L1·Co@NH$_3$** have three excitations with oscillator strength greater than 0.1 in their main absorption. To assign the characteristics of these excitations, natural transition orbital (NTO) analyses[33] were performed. In **L1·Co**, although the ILCT transition is still present, MLCT dominates one of these excitations (*ca.* 38%), thereby suppressing the ILCT contribution and quenching the luminescence (Fig. S4). Upon exposure to $NH_3$ vapor, the electronic structure of **L1·Co@NH$_3$** shifts back toward an ILCT-dominant excited state (Fig. S5). This result indicates that $NH_3$ coordination likely weakens the competing MLCT pathway, thereby enabling the re-emergence of ILCT-driven luminescence. Besides, although the emission of **L1·Co@NH$_3$** originates predominantly from a ligand-centered excited state, additional nonradiative relaxation pathways associated with the cobalt(II) center are still operative. It should be noted that the present TD-DFT calculations primarily describe ligand- or metal-centered charge-transfer, whereas the d–d states are not explicitly described within this computational operation.

Photoluminescence lifetime measurements were performed to further elucidate the optical response (Fig. S6 and Table S3). The decay profile of the free ligand **L1** (green plots) displays lifetimes of $\tau_1$ = 0.34 ns and $\tau_2$ = 1.06 ns, whereas that of the cobalt(II) complex after $NH_3$ exposure, **L1·Co@NH$_3$** (red plots), exhibits longer lifetimes of $\tau_1$ = 0.56 ns and $\tau_2$ = 2.51 ns. In contrast, pristine **L1·Co** without $NH_3$ exposure does not show a detectable lifetime owing to the absence of observable luminescence. Considering that the ligand is only partially dissociated from the central Co(II) ion upon $NH_3$ coordination, rather than being fully released, the observed lifetimes—distinct from those of free **L1**—are reasonable.

In addition to the spectroscopic observations and DFT results, the response mechanism toward $NH_3$ vapor was investigated by elemental analysis, PXRD, gas adsorption isotherms, and thermogravimetric analysis (TGA). After exposure of **L1·Co** to $NH_3$ vapor, elemental analysis revealed a marked increase in nitrogen content for **L1·Co@NH$_3$**, indicating the uptake of $NH_3$ molecules (+$H_2O$ and +5.5$NH_3$, Table S2). The $NH_3$ adsorption isotherm measured at 25 °C shows a gradual uptake at lower pressures, followed by a steep increase beginning at $P_{NH_3}$ = 21 kPa, indicative of gate-opening (GO) adsorption behavior, to reach an adsorption amount of 211 mL (stp) $g^{-1}$ (5.4 mol per formula unit) at 100 kPa (Fig. S7). This is in good agreement with the results of elemental analysis for **L1·Co@NH$_3$**.

On the other hand, the PXRD pattern of **L1·Co@NH$_3$** differs from that of pristine **L1·Co** after exposure to $NH_3$ vapor (Fig. 3). That is, the optical change caused by $NH_3$ vapor is

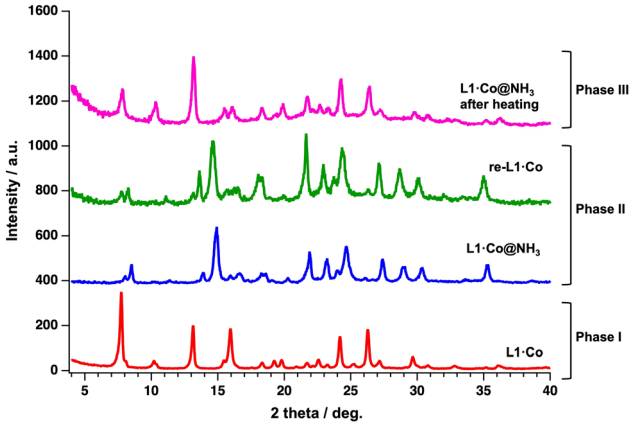


Fig. 3 PXRD patterns of **L1·Co** (red), **L1·Co@NH$_3$** (blue), **re-L1·Co** (green) and **L1·Co@NH$_3$** after thermal treatment (magenta), $\lambda$ = 1.54 Å.

accompanied by a structural change due to the GO adsorption behavior. Notably, the PXRD pattern of **re-L1·Co** is nearly identical to that of **L1·Co@NH$_3$**, even though its optical properties revert toward those of pristine **L1·Co**. Elemental analysis of **re-L1·Co** dried for 3 h indicates the presence of a small portion of residual $NH_3$ molecules (+1.8$H_2O$ and +2.8$NH_3$, Table S2). After further air-drying for 1 and 3 days, CHN analysis showed no significant change compared to the 3 h dried sample, remaining within experimental uncertainty. This indicates that $NH_3$ desorption predominantly occurs within the initial 3 h, with approximately 3 mol released before reaching a steady composition. Nevertheless, the reflectance spectra clearly indicate re-coordination of **L1** to the Co(II) center, demonstrating that the residual $NH_3$ molecules remaining in **re-L1·Co** are adsorbed in a coordination-free manner or replace chloride ions, rather than being directly bound to the metal center. Furthermore, TGA of **L1·Co@NH$_3$** shows a weight loss of *ca.*13% upon heating to 450 K (Fig. S8), which is consistent with the release of 0.5 $H_2O$ and 5 $NH_3$ molecules. Elemental analysis of **L1·Co@NH$_3$** after thermal treatment at 450 K indicates the presence of residual 0.5$H_2O$ and 0.5$NH_3$ molecules (bottom in Table S2). The PXRD pattern of the thermally treated **L1·Co@NH$_3$** is identical to that of pristine **L1·Co**, indicating recovery of the original crystal structure. However, a slight shift of the main diffraction peak toward higher 2$\theta$ (7.72° for **L1·Co** and 7.84° for thermally treated **L1·Co@NH$_3$**) suggests a minor lattice contraction. Although the overall diffraction pattern closely resembles that of pristine **L1·Co**, such subtle densification may reduce the local free volume and/or diffusion pathways required for guest uptake, potentially leading to reduced responsiveness.[34,35] This effect is therefore more likely associated with bulk structural contraction rather than solely with residual guest molecules adsorbed on the surface.

Fig. 4 presents a schematic illustration of the $NH_3$ vapor responsivity of **L1·Co**, in which each state is categorized as Phases I–III. The corresponding phases are also reflected in the PXRD patterns shown in Fig. 3. As described above, pristine **L1·Co** exhibits no luminescence and is defined as Phase I. In Phase II, **L1·Co@NH$_3$** and **re-L1·Co** reversibly interconvert, accompanied by distinct color changes and luminescence ON–OFF switching.

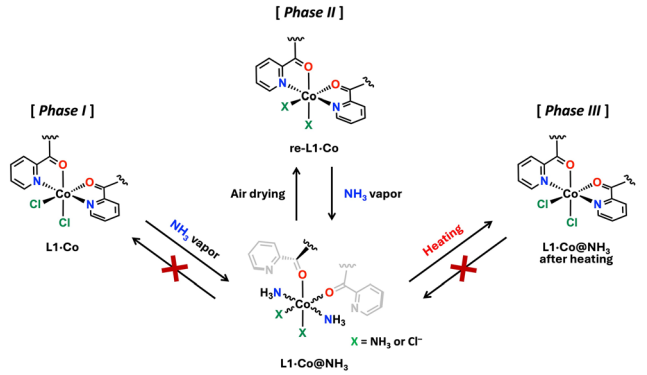


Fig. 4 Schematic diagram of $NH_3$ vapor responsivity of **L1·Co** focusing on the coordination geometry. Phase I: The pristine **L1·Co** with no luminescent activity. Phase II: **L1·Co@NH$_3$** and **re-L1·Co** with reversible luminescent ON–OFF behavior. Phase III: Thermally treated **L1·Co@NH$_3$** with no luminescent activity.

The exact coordination environment at the Co(II) center in Phase II cannot be unambiguously determined. Therefore, we propose a plausible coordination model (X = $NH_3$ or $Cl^-$) consistent with elemental analysis, spectroscopic data, and PXRD results. Elemental analysis indicates the presence of two chloride ions, suggesting that $Cl^-$ remains in the lattice as counter anions even when $NH_3$ coordinates to the metal center. A small amount of $NH_3$ also persists after drying **L1·Co@NH$_3$** without significant structural change, as supported by PXRD. These residual $NH_3$ molecules are likely involved in maintaining the reversible optical response of Phase II. In contrast, thermal treatment of **L1·Co@NH$_3$** generates Phase III, in which the original PXRD pattern of **L1·Co** is restored, while approximately 0.5 mol of $NH_3$ and $H_2O$ remain in the material. Unlike Phase II, the presence of these residual guest molecules in Phase III likely hinders further $NH_3$ uptake, thereby suppressing the coordination-driven optical response.

In conclusion, we have demonstrated that a structurally defined chalcone-based Co(II) complex exhibits highly selective and reversible vapochromism together with luminescence ON–OFF switching in response to $NH_3$ vapor. A combination of spectroscopic measurements, PXRD, gas adsorption analysis, and DFT calculations strongly suggests that this behavior most likely originates from a coordination-driven switching process involving partial ligand dissociation and reversible $NH_3$ binding. The present study highlights a molecular design for fast and selective vapor sensing based on the reversible metal–ligand reconfiguration in discrete coordination compounds.

## Conflicts of interest

There are no conflicts to declare.

## Data availability

The data supporting the results of this study have been included in the supplementary information (SI). See DOI: https://doi.org/10.1039/d5cc07385e.

CCDC 2512162 contains the supplementary crystallographic data for this paper.[36]

## Acknowledgements

This work was supported by a JSPS KAKENHI Grant-in-Aid for Early-Career Scientists (No. JP22K14695). M. N. also acknowledges financial support from the Iketani Science and Technology Foundation (ISTF, No. 0351080-A) and the Kurita Water and Environment Foundation (No. 25H015).

## References

1 A. Fernández-Acebes and J.-M. Lehn, *Chem. – Eur. J.*, 1999, **5**, 3285.
2 Q. Zhao, F. Li and C. Huang, *Chem. Soc. Rev.*, 2010, **39**, 3007.
3 P. Hajivand, J. C. Jansen, E. Pardo, D. Armentano, T. F. Mastropietro and A. Azadmehr, *Coord. Chem. Rev.*, 2024, **501**, 215558.
4 N. Dey, D. Biswakarma and S. Bhattacharya, *ACS Sustainable Chem. Eng.*, 2019, **7**, 569.
5 S. Fujii, H. Yagi, T. Kawaguchi, M. Ishikawa, N. Izumiyama and M. Nakaya, *Dalton Trans.*, 2023, **52**, 10206.
6 S. Khanra, M. Sahad E, S. Das, S. Chakraborty, P. Brandao, B. de Bruin, B. C. Das and N. D. Paul, *Adv. Funct. Mater.*, 2025, **35**, 2502728.
7 P. Sarkar, L. T. Manamel, P. Saha, C. Jana, A. Sarmah, K. U. Mohanan, B. C. Das and C. Mukherjee, *Mater. Horiz.*, 2025, **12**, 246.
8 S. Sinha, M. Sahad E, R. Mondal, S. Das, L. T. Manamel, P. Brandão, B. de Bruin, B. C. Das and N. D. Paul, *J. Am. Chem. Soc.*, 2022, **144**, 20442.
9 R. Mondal, A. K. Guin, S. Chakraborty and N. D. Paul, *J. Org. Chem.*, 2022, **87**, 2921.
10 D. Sengupta, S. Goswami, R. Banerjee, M. J. Guberman-Pfeffer, A. Patra, A. Dutta, R. Pramanick, S. Narasimhan, N. Pradhan, V. Batista, T. Venkatesan and S. Goswami, *Chem. Sci.*, 2020, **11**, 9226.
11 S. A. Hilderbrand, M. H. Lim and S. J. Lippard, *J. Am. Chem. Soc.*, 2004, **126**, 4972.
12 M. H. Lim and S. J. Lippard, *J. Am. Chem. Soc.*, 2005, **127**, 12170.
13 X. Zhang, B. Li, Z.-H. Chen and Z.-N. Chen, *J. Mater. Chem.*, 2012, **22**, 11427.
14 D. Saito, T. Galica, E. Nishibori, M. Yoshida, A. Kobayashi and M. Kato, *Chem. – Eur. J.*, 2022, **28**, e202200703.
15 Y. Shen, A. Tissot and C. Serre, *Chem. Sci.*, 2022, **13**, 13978.
16 H. Yuan, N. Li, W. Fan, H. Cai and D. Zhao, *Adv. Sci.*, 2022, **9**, 2104374.
17 Z. Gao, Y. Lai, Y. Tao, L. Xiao, L. Zhang and F. Luo, *ACS Cent. Sci.*, 2021, **7**, 1066.
18 P. Qin, B. A. Day, S. Okur, C. Li, A. Chandresh, C. E. Wilmer and L. Heinke, *ACS Sens.*, 2022, **7**, 1666.
19 S. Wang, Y. Fu, T. Wang, W. Liu, J. Wang, P. Zhao, H. Ma, Y. Chen, P. Cheng and Z. Zhang, *Nat. Commun.*, 2023, **14**, 7261.
20 H. Yoshino, M. Saigo, T. Ehara, K. Miyata, K. Onda, J. Pirillo, Y. Hijikata, S. Takaishi, W. Kosaka, K. Otake, S. Kitagawa and H. Miyasaka, *Angew. Chem., Int. Ed.*, 2025, **64**, e202413830.
21 A. Tiwari, M. Arjumanda and A. Yella, *Nanoscale*, 2024, **16**, 22152.
22 O. S. Wenger, *Chem. Rev.*, 2013, **113**, 3686.
23 P. Kar, M. Yoshida, Y. Shigeta, A. Usui, A. Kobayashi, T. Minamidate, N. Matsunaga and M. Kato, *Angew. Chem., Int. Ed.*, 2017, **56**, 2345.
24 S. Kusumoto, K. Inaba, H. Suda, M. Nakaya, R. Tokunaga, P. Thuéry, R. Haruki, T. Kanazawa, S. Nozawa, Y. Kim, S. Hayami and Y. Koide, *Inorg. Chem.*, 2023, **62**, 16222.
25 T. Murakami, A. Masuno, M. Okazaki and S. Ohta, *Inorg. Chem.*, 2025, **64**, 15332.
26 O. Baumeyer, A. Wu, A. Pandya, P. Nelson, P. C. Hillesheim, M. Zeller, G. M. Carignan, J. Li and D. W. Ki, *Chem. Commun.*, 2025, **61**, 10170.
27 J. M. Len, N. Hussein, S. Malla, K. Mcintosh, R. Patidar, M. Elangovan, K. Chandrabose, N. S. H. N. Moorthy, M. Pandey, D. Raman, P. Trivedi and A. K. Tiwari, *Molecules*, 2021, **26**, 4214.
28 R. Sander, *Atmos. Chem. Phys.*, 2023, **23**, 10901.
29 B. E. R. Snyder, A. B. Turkiewicz, H. Furukawa, M. V. Paley, E. O. Velasquez, M. N. Dods and J. R. Long, *Nature*, 2023, **613**, 287.
30 E. D. Raczyńska, J.-F. Gal and P.-C. Maria, *Int. J. Mass Spectrom.*, 2017, **418**, 130.
31 A. D. Becke, *J. Chem. Phys.*, 1993, **98**, 5648.

32 M. J. Frisch, G. W. Trucks, H. B. Schlegel, G. E. Scuseria, M. A. Robb, J. R. Cheeseman, G. Scalmani, V. Barone, G. A. Petersson, H. Nakatsuji, X. Li, M. Caricato, A. V. Marenich, J. Bloino, B. G. Janesko, R. Gomperts, B. Mennucci, H. P. Hratchian, J. V. Ortiz, A. F. Izmaylov, J. L. Sonnenberg, D. Williams-young, F. Ding, F. Lipparini, F. Egidi, J. Goings, B. Peng, A. Petrone, T. Henderson, D. Ranasinghe, V. G. Zakrzewski, J. Gao, N. Rega, G. Zheng, W. Liang, M. Hada, M. Ehara, K. Toyota, R. Fukuda, J. Hasegawa, M. Ishida, T. Nakajima, Y. Honda, O. Kitao, H. Nakai, T. Vreven, K. Throssell, J. A. Montgomery Jr., J. E. Peralta, F. Ogliaro, M. J. Bearpark, J. J. Heyd, E. N. Brothers, K. N. Kudin, V. N. Staroverov, T. A. Keith, R. Kobayashi, J. Normand, K. Raghavachari, A. P. Rendell, J. C. Burant, S. S. Iyengar, J. Tomasi, M. Cossi, J. M. Millam, M. Klene, C. Adamo, R. Cammi, J. W. Ochterski, R. L. Martin, K. Morokuma, O. Farkas, J. B. Foresman and D. J. Fox, *Gaussian 16, Revision C.01*, Gaussian, Inc., Wallingford CT, 2016.
33 R. L. Martin, *J. Chem. Phys.*, 2003, **118**, 4775.
34 J. E. Mann, R. Gao, S. S. London and J. A. Swift, *Mol. Pharmaceutics*, 2023, **20**, 5554.
35 A. Yao, H. Xu, K. Shao, C. Sun, C. Qin, X. Wang and Z. Su, *Nat. Commun.*, 2025, **16**, 1385.
36 CCDC 2512162: Experimental Crystal Structure Determination, 2026, DOI: 10.5517/ccdc.csd.cc2qb3hp.